Application of the hyperspherical hidden-crossing method to positronium formation in positron-lithium collisions

S. J. Ward
Department of Physics, University of North Texas, Denton, Texas 76203, USA

J. Shertzer
Department of Physics, College of the Holy Cross, Worcester, Massachusetts 01610, USA

(Received 28 March 2003; published 29 September 2003)

The hyperspherical hidden-crossing method (HHCM) has been applied to *s*-, *p*-, and *d*-wave positronium formation in positron-lithium collisions in the energy range 0–1.8 eV, using a model potential to describe the atomic core. The calculations have provided a test of the HHCM. The *s*-, *p*-, and *d*-wave positronium formation cross sections are reported and compared with variational and close-coupling calculations. A minimum is obtained in the *s*-wave positronium formation cross section which is due to the Stuckelberg phase having a value of π. The cross sections have also been computed including the correction term which emerges from the one-Sturmian theory.

DOI: 10.1103/PhysRevA.68.032720 PACS number(s): 34.85.+x

I. INTRODUCTION

Low-energy positron-lithium collisions are of interest because the ground-state positronium formation channel is open even at zero incident positron energy. The ionization energy of lithium (5.4 eV) [1] is smaller than the binding energy of positronium (6.8 eV). According to Wigner's threshold law [2], the *s*-wave positronium formation cross section is infinite at zero incident positron energy. Lithium can be approximated as an one-electron atom which means that positron-lithium collisions can be considered as an effective three-body system.

A. Previous experimental measurements and calculations of positronium formation in $e^+ + \mathrm{Li}$ collisions

Recently, Surdutovich *et al.* [3] measured the positronium formation cross section for positron-lithium collisions for energies down to a few tenths of an electron volt. There have been several calculations of the positronium formation cross section but relatively few for low energy.

Watts and Humberston [4–6] employed the Kohn variational method to compute the *s*-, *p*-, and *d*-wave positronium formation cross sections for positron-lithium collisions in the energy range 0–1.8 eV where there are only two open channels, elastic scattering and ground-state positronium formation. They reported that the *s*-wave positronium formation cross section decreased as the number of terms in the trial function was increased [6].

A pioneering calculation of the positronium formation cross section in the energy range 0.5–10 eV was performed by Guha and Ghosh [7] using a two-state $\mathrm{Li}(2s)+\mathrm{Ps}(1s)$ close-coupling approximation (CCA). Later, Basu and Ghosh [8] used a three-state $\mathrm{Li}(2s,2p)+\mathrm{Ps}(1s)$ CCA to compute the positronium formation cross section for energies up to 100 eV. Hewitt *et al.* [9,10] considered the $\mathrm{Li}(2s,2p,3s,3p)+\mathrm{Ps}(1s,2s,2p)$ CCA for positron-lithium collisions for energies up to 50 eV.

Kernoghan *et al.* [11] performed a number of CCA calculations for the *s*-, *p*-, and *d*-wave positronium formation cross section for energies up to 2.8 eV. They varied the number of target atomic states, positronium atomic states, and pseudostates in the expansion of the wave function. Their most elaborate calculation is a 14-state $\mathrm{Ps}(1s,2s,3\bar{s},4\bar{s},2p,3\bar{p},4\bar{p},3\bar{d},4\bar{d})+\mathrm{Li}(2s,2p,3s,3p,3d)$ CCA. For the *s* wave, there is some discrepancy between the 14-state CCA and the variational results, but the cross sections are the same order of magnitude and good agreement is achieved at energies above 1.6 eV. For the *p* wave, the 14-state CCA and variational results agree well for the entire energy range.

McAlinden *et al.* [12] have extended the 14-state CCA calculation of Kernoghan *et al.* [11] to higher energies (0.5–60 eV) and have also performed a 32-state CCA calculation. The 32-state CCA includes 3 positronium states and 29 lithium atomic and pseudostates. There is good agreement between the 14-state CCA and the 32-state CCA for the ground-state positronium formation cross section (summed over partial waves). The total positronium formation cross section agrees with experimental measurements [3].

B. Previous calculations using the hyperspherical hidden-crossing method

The hyperspherical hidden-crossing method (HHCM) was formulated to treat the correlated motion of three charged particles of arbitrary mass and charge [13]. A significant feature of HHCM is that it can give rise to an interpretation of a scattering process. For instance, the HHCM calculations of the *s*-, *p*-, and *d*-wave positronium formation cross sections for positron-hydrogen collisions in the Ore gap provided an explanation for the small *s*-wave and large *d*-wave positronium formation cross sections [14]. For the *s* wave, the Stuckelberg phase is close to π and the two amplitudes that correspond to different paths leading to positronium formation interfere destructively. In contrast, for the *d* wave, the Stuckelberg phase is close to $\pi/2$ and the two amplitudes interfere constructively. The HHCM has also provided an

 ©2003 The American Physical Society

interpretation of the the minimum in the transition probability for the reaction $^4He+^4He+^4He \rightarrow ^4He+^4He_2$ [15], which occurs at an energy where the Stuckelberg phase is 3π.

Despite the success of HHCM in giving an interpretation of scattering processes, there have only been a limited number of applications [13–21] of the method since its formulation. The method is not exact, and needs to be further tested to determine its accuracy in describing collisions involving three particles. With this goal in mind, we have applied the HHCM to positronium formation for low-energy positron collisions with lithium. Although formulated for three-body systems, the method is readily extended to positron-lithium collisions by incorporating a model potential to describe the atomic core.

In Sec. II, we present a summary of the formulation of the HHCM and provide details on the model potential. In Sec. III, we discuss the computational tools which we developed specifically for the application of the HHCM to low-energy positron collisions. In Sec. IV, we present the *s*-, *p*-, and *d*-wave positronium formation cross sections for positron-lithium collisions; we compare the HHCM results with variational and CCA results and discuss the importance of the Stuckelberg phase. In Sec. V, we give the conclusion and the long term goal of the HHCM study of positron–alkali-metal collisions.

Atomic units are used throughout unless explicitly stated.

II. HYPERSPHERICAL HIDDEN-CROSSING METHOD

The original hidden-crossing theory developed by Landau [22] for ion-atom collisions used a semiclassical approximation for internuclear motion. Macek and Ovchinnikov [13] derived a hidden-crossing theory without the semiclassical approximation, thus extending the applicability to three charged particles of arbitrary mass. Their derivation is based on the hyperspherical representation. The theory is summarized below for positron-hydrogen collisions; the application of the hidden-crossing method to positron-lithium collisions is discussed at the end of this section.

The hyperspherical coordinates are the hyper-radius $R=\sqrt{r_1^2+r_2^2}$ and the hyperangles $\alpha=\tan^{-1}(r_2/r_1)$ and $\theta=\cos^{-1}(\hat{\mathbf{r}}_1\cdot\hat{\mathbf{r}}_2)$, where $\mathbf{r}_1$ and $\mathbf{r}_2$ are the position vectors of e^+ and e^- with respect to the (infinitely heavy) proton [23]. The reduced wave function $\Psi(R,\Omega)$ is related to the Schrödinger wave function $\psi(R,\Omega)$ by $\Psi(R,\Omega)=R^{5/2}\sin\alpha\cos\alpha\,\psi(R,\Omega)$ [23], where Ω represents the hyperangles α, θ, and the three Euler angles. The Schrödinger equation is expressed as

$$\left[-\frac{\partial^2}{\partial R^2}+\frac{\Lambda^2+2RC(\Omega)}{R^2}-2E\right]\Psi(R,\Omega)=0, \tag{1}$$

where

$$\Lambda^2=-\frac{\partial^2}{\partial\alpha^2}+\frac{\mathbf{L}_1^2}{\cos^2\alpha}+\frac{\mathbf{L}_2^2}{\sin^2\alpha}-\frac{1}{4} \tag{2}$$

and

$$C(\Omega)=-\frac{1}{\sin\alpha}+\frac{1}{\cos\alpha}-\frac{1}{\sqrt{1-\sin 2\alpha\cos\theta}}. \tag{3}$$

The hyperspherical adiabatic basis functions $\varphi_\mu(R;\Omega)$ are found by holding R fixed and solving

$$[\Lambda^2+2RC(\Omega)]\varphi_\mu(R;\Omega)=2\varepsilon_\mu(R)R^2\varphi_\mu(R;\Omega) \tag{4}$$

for the adiabatic energy eigenvalues $\varepsilon_\mu(R)$. Alternatively, the angle-Sturmian basis functions $S_n(\nu;\Omega)$ are found by holding $(\nu^2-\frac{1}{4})$ fixed and solving

$$[\Lambda^2+2\rho_n(\nu)C(\Omega)]S_n(\nu;\Omega)=(\nu^2-\tfrac{1}{4})S_n(\nu;\Omega) \tag{5}$$

for the eigenvalues $\rho_n(\nu)$. The adiabatic energy eigenvalues $\varepsilon_\mu(R)$ correspond to different branches on the real axis of the function $\varepsilon(R)$, which is single-valued function on a Riemann surface [13,24]. The sheets are joined at branch points in the complex plane, and different sheets can be reached by circling a branch point. Since $\varepsilon(R)$ is defined for all R, when $2\varepsilon(\rho)\rho^2=\nu^2-\frac{1}{4}$, the Sturmian eigenfunction $S_n(\nu;\Omega)$ is equal to the adiabatic function $\varphi(R=\rho(\nu);\Omega)$ to within a normalization constant.

The exact wave function $\Psi(R,\Omega)$ for three charged particles can be expressed as

$$\Psi(R,\Omega)=\int_c\sqrt{R}Z_\nu(KR)\Phi(\nu,\Omega)2\nu d\nu, \tag{6}$$

where $Z_\nu(KR)$ are Bessel functions of total energy $E=K^2/2$ and c denotes a contour in the ν plane. The unknown coefficients $\Phi(\nu,\Omega)$ can be expanded in the angle Sturmian basis functions. The hidden-crossing theory emerges by truncating the expansion to a single-Sturmian function, taking the asymptotic limit $(R\rightarrow\infty)$ of the wave function, and evaluating the integral using stationary phase approximation. The resulting wave equation (see Ref. [13] for details), aside from an unimportant multiplicative factor, is given by

$$\Psi(R,\Omega)\approx\sum_{paths}\sum_{\mu}\frac{1}{\sqrt{K_\mu(R)}}\times\exp\left(i\int_{c_\mu}^{R}K_\mu(R')dR'\right)\varphi_\mu(R;\Omega),\quad R\rightarrow\infty, \tag{7}$$

where

$$K_\mu^2(R)=K^2-2\varepsilon'_\mu(R) \tag{8}$$

and

$$\varepsilon'_\mu(R)=\varepsilon_\mu(R)+\frac{1}{2}\left(\frac{1}{4R^2}\right). \tag{9}$$

Note that the wave function $\Psi(R,\Omega)$ of Eq. (7) is of the WKB form even though no semiclassical approximation was made at the outset.

To apply the HHCM, one must compute the wave vector $K_\mu(R)$. Following Zhou and Lin [23], the adiabatic function $\varphi(R;\Omega)$ is expanded into states of total angular momentum L:

$$\varphi_\mu(R;\Omega)=\sum_{I=0}^{L} f_I(R;\alpha,\theta)\mathcal{D}^{(L)}_{|I|,M}(\omega_1,\omega_2,\omega_3), \quad (10)$$

where $\omega_1,\omega_2,\omega_3$ are the three Euler angles. The functions $f_I(R;\alpha,\theta)$ are solutions to the coupled partial differential equations

$$\sum_{J=0}^{L} \mathcal{H}_{I,J} f_J(R;\alpha,\theta)=2R^2\varepsilon'_\mu(R) f_I(R;\alpha,\theta),$$

$$I=0,1,2,\ldots,L, \quad (11)$$

where the operators $\mathcal{H}_{I,J}$ are given in Refs. [23,25]. The eigenvalues $\varepsilon'_\mu(R)$ [14] can then be used to calculate the wave vector $K_\mu(R)$ for the Lth partial wave. (The L superscript for the wave vector and eigenvalues has been suppressed for brevity).

The Jost matrix for the Lth partial wave is obtained from the asymptotic form of the wave function. The S-matrix element for a transition between two adjacent levels i and j is given by

$$S^L_{ij}=[(J^-)^{-1}]_{ii}J^+_{ij}+[(J^-)^{-1}]_{ij}J^+_{jj}. \quad (12)$$

The modulus square of the S-matrix element $|S^L_{ij}|^2$ can be expressed in the form

$$|S^L_{ij}|^2=4P^L_{ij}\sin^2\Delta^L_{ij}, \quad (13)$$

where

$$\Delta^L_{ij}=\left|\mathrm{Re}\left[\int_c K(R)dR\right]\right|,$$

$$P^L_{ij}=\exp\left(-2\left|\mathrm{Im}\left[\int_c K(R)dR\right]\right|\right). \quad (14)$$

In Eq. (14), Δ^L_{ij} is the Stuckelberg phase and P^L_{ij} is the one-way transition probability. The contour c is from the classical turning point R^t_i on the sheet of the Riemann surface corresponding to level i, around the branch point R_b, to the classical turning point R^t_j on the sheet corresponding to level j. The S matrix of Eq. (13) does not satisfy unitarity. To ensure unitarity, Eq. (13) is multiplied by the factor $(1-P^L_{ij})$ to give

$$|\tilde{S}^L_{ij}|^2=4P^L_{ij}(1-P^L_{ij})\sin^2\Delta^L_{ij}. \quad (15)$$

The justification for the factor $(1-P^L_{ij})$ can be found in Refs. [26,27]. The partial wave cross section for the transition between two levels (in units of πa_0^2)

$$\sigma^L_{ij}=\frac{(2L+1)}{k_i^2}|\tilde{S}^L_{ij}|^2, \quad (16)$$

where k_i is the incident momentum.

Within the framework of the one-Sturmian theory, one can calculate a correction to the wave vector for large R where $\varepsilon(R)$ is a slowly varying function of R [13,14]. The corrected wave vector $\tilde{K}^2_\mu(R)$ is given by

$$\tilde{K}^2_\mu(R)=K^2-2\tilde{\varepsilon}'_\mu(R), \quad (17)$$

where

$$\tilde{\varepsilon}'_\mu(R)=\varepsilon'_\mu(R)-\frac{1}{2}\left[\frac{1}{4R^2}+\left\langle\varphi_\mu\left|\frac{\partial^2\varphi_\mu}{\partial R^2}\right\rangle\right.\right]$$

$$=\varepsilon_\mu(R)-\frac{1}{2}\left\langle\varphi_\mu\left|\frac{\partial^2\varphi_\mu}{\partial R^2}\right\rangle\right. . \quad (18)$$

It has been shown that the potential $\tilde{\varepsilon}'_\mu(R)$ asymptotically gives the close-coupling channel potentials through terms of the order of $1/R^2$ [28–30].

The HHCM can be applied to positron-lithium collisions by using model potentials. We chose the same model potential as used in the variational calculation [4–6] to allow a more direct comparison of results. The model potential is of the form given by Peach [31] but without the core-polarization term. The electron-core interaction is

$$V_{e^-\mathrm{Li}^+}=-\frac{1}{r}-\frac{2}{r}e^{-\gamma r}(1+\delta r+\delta' r^2). \quad (19)$$

The values of the parameters are given in Ref. [5] and were chosen to fit spectroscopic data. The potential also supports a bound $1s$ state (-51.5 eV) which is unphysical but well separated in energy from the ground-state Li($2s$) (-5.39 eV). The positron-core interaction is taken to be the negative of the static interaction Eq. (19). Unlike the hydrogenic case, the reduced potential,

$$C(R;\alpha,\theta)$$

$$=\frac{1}{\cos\alpha}[1+2e^{-\gamma R\cos\alpha}(1+\delta R\cos\alpha+\delta' R^2\cos^2\alpha)]$$

$$-\frac{1}{\sin\alpha}[1+2e^{-\gamma R\sin\alpha}(1+\delta R\sin\alpha+\delta' R^2\sin^2\alpha)]$$

$$-\frac{1}{[1-\sin 2\alpha\cos\theta]^{1/2}}, \quad (20)$$

depends upon the parameter R.

III. COMPUTATIONAL TOOLS

To apply the HHCM to s-, p-, and d-wave positron-lithium scattering, it is necessary to solve the hyperspherical coupled partial differential equations, Eq. (11), for the lowest eigenvalues at thousands of values of R, real and complex. The eigenvalues need to be obtained to a high accuracy: a few parts in 10^6 for small R and a few parts in 10^4 for large R. We developed two numerical tools to compute the eigenvalues accurately and efficiently. First, we wrote finite ele-

ment method (FEM) codes to solve the hyperspherical coupled partial differential equations for $L=0,1$, and 2 [32]. Second, we developed a vector iteration program for the eigenvalue equation.

The FEM is ideally suited for hyperspherical calculations of Coulomb systems [33]. The use of local interpolation allows one to concentrate the polynomial basis functions in the region of the potential singularities, which include an attractive line singularity at $\alpha=0$, a repulsive line singularity at $\alpha=\pi/2$, and an attractive point singularity at $\theta=0,\alpha=\pi/4$. Although the FEM polynomials guarantee continuity of the function $\Psi(R;\alpha,\theta)$ and its derivatives $\partial\Psi/\partial\alpha$ and $\partial\Psi/\partial\theta$ across the element interfaces, it is possible to relax this condition and allow the derivative $\partial\Psi/\partial\alpha$ to be discontinuous at the point singularity. Although this modification is not particularly important at small R, it improves significantly the accuracy of the energy at large R, where the cusp in the wave function is extremely sharp and narrow.

Most of the CPU time in the HHCM calculation is spent in solving the resulting eigenvalue problem. In FEM, one obtains a banded generalized eigenvalue matrix equation; only the lowest few eigenvalues are needed. The matrix is complex for complex R. We developed a code to solve the real/complex generalized eigenvalue problem in banded storage mode using vector iteration. The rate of convergence of vector iteration depends on the accuracy of the initial guesses of the eigenvalue and eigenvector.

The exact eigenvalues and eigenvectors are known for $R=0$. Since some of the levels are degenerate at $R=0$, it is important to split the degeneracy and order the levels correctly for the first nonzero R point on the real axis. In this case, our input into the vector iteration is the exact eigenvalues at $R=0$ (plus a correction obtained from first-order perturbation theory) and the exact analytical eigenfunctions. At each additional point on the real axis, we input the eigenvalues [plus a correction term $(\Delta E/\Delta R\cdot\Delta R)$] and eigenvectors from the previous value of R. In all cases, we obtained eight digit convergence in just two or three iterations. We compute the eigenvalues up to large $R=80$ a.u. in order to identify which physical channel is associated with each of the eigenvalues. This also enables us to to check the accuracy of the eigenvalues at large R by comparing the computed eigenvalues with the known values of the bound-state energies of the ground and excited states of lithium and positronium.

The next step is to locate the branch point that connects the two sheets whose eigenvalues asymptotically correspond to the physical levels of $e^+ + \mathrm{Li}(2s)$ and $\mathrm{Ps}(1s)+\mathrm{Li}^+$. As one goes around a closed path that encloses this branch point, the eigenvalues associated with these two sheets interchange. Because we are inputting both an initial eigenvalue and eigenvector into the vector iteration, there is no ambiguity about the ordering of the complex eigenvalues. We can obtain the position of the branch point to the desired accuracy by systematically decreasing the size of the closed path.

IV. RESULTS

Using the HHCM with the model potential given by Eqs. (19) and (20), we calculated the *s*-, *p*-, and *d*-wave positronium formation cross sections for $e^+ + \mathrm{Li}$ collisions in the energy range 0–1.8 eV. We computed along the real axis $(0\leqslant R\leqslant 80)$ the lowest three potentials $\varepsilon'_\mu(R)$ for the *s*, *p*, and *d* waves. Figure 1 is a plot of the potentials $\varepsilon'_\mu(R)$ for the *s* wave. The lowest three eigenvalues $\varepsilon'_\mu(R)$ for each partial wave asymptotically approach $\mathrm{Li}(1s)$, $\mathrm{Ps}(1s)$, and $\mathrm{Li}(2s)$, respectively.

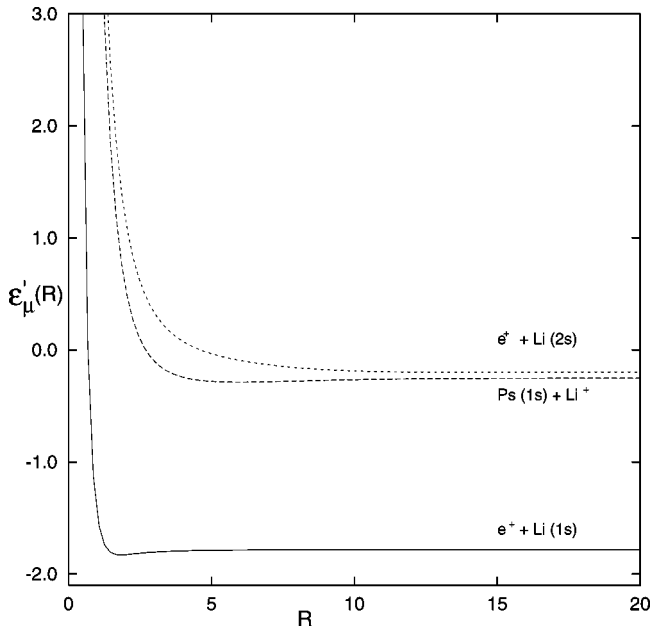

FIG. 1. The lowest three $\varepsilon'_\mu(R)$ potentials for $L=0$.

For each partial wave, we located as a function of energy the classical turning points R_2^t and R_3^t on the second and third potential curves and the branch point R_{23}^b that connects eigenvalues $\varepsilon'_2(R)$ and $\varepsilon'_3(R)$. For the *s* and *p* waves, the branch point is at $R_{23}^b=10.80+i4.80$ and for the *d* wave at $R_{23}^b=10.65+i4.95$. The real part of the position of this branch point for each partial wave is to the right of R_2^t.

We also found another branch point connecting $\varepsilon'_2(R)$ and $\varepsilon'_3(R)$ much closer to the origin. It is likely due to the use of model potentials rather than a pure Coulomb potential. However, because $\mathrm{Re}(R_{23}^b)<R_2^t$ a transition can only be made from the $\varepsilon'_2(R)$ to $\varepsilon'_3(R)$ around this branch point via tunneling. It is therefore a reasonable approximation to neglect this branch point. We also located a branch point that connects eigenvalues $\varepsilon'_1(R)$ and $\varepsilon'_2(R)$ for the *s* wave and a branch point that connects eigenvalues $\varepsilon'_1(R)$ and $\varepsilon'_3(R)$ for the *p* wave. The real part of the position of these branch points is less than R_2^t and R_3^t, and for the same reason we neglected them in the calculations.

For each partial wave, we computed the contour integral of Eq. (14) where the contour c is from R_2^t around the branch point R_{23}^b to R_3^t. Using this contour integration, we computed the Stuckelberg phase and probability according to Eq. (14) and the modulus squared of the *S*-matrix element $\tilde{S}_{23}^L$ for the transition $\mathrm{Ps}(1s)+\mathrm{Li}^+\rightarrow e^+ + \mathrm{Li}(2s)$ according to Eq. (15). The *S*-matrix element $\tilde{S}_{32}^L$ for ground-state positronium formation is equal to this *S*-matrix element $\tilde{S}_{23}^L$. From $|\tilde{S}_{32}^L|^2$,

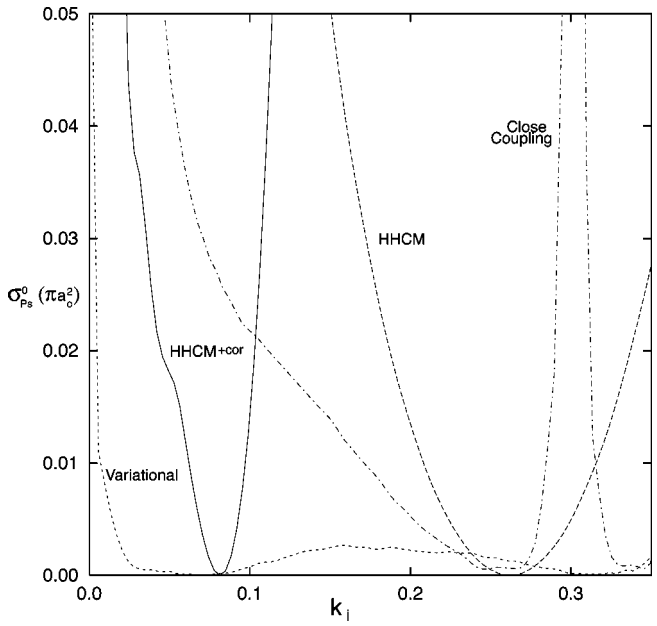

FIG. 2. The *s*-wave positronium formation cross section for $e^+ + \mathrm{Li}$ collisions computed by the HHCM (long-dashed), the $\mathrm{HHCM}^{+\mathrm{cor}}$ (solid), the variational method (short-dashed) [4–6], and the 14-state CCA (dot-dashed) [11]. The variational and 14-state CCA results are from the figures in Ref. [5].

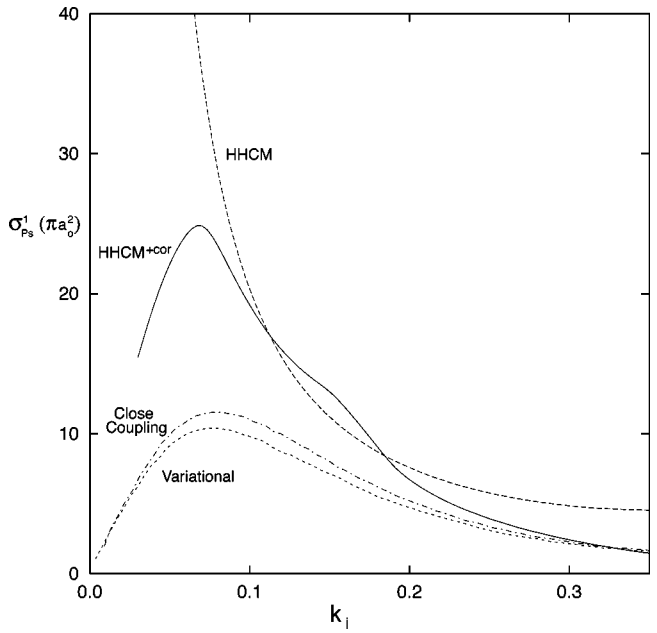

FIG. 3. The *p*-wave positronium formation cross section for $e^+ + \mathrm{Li}$ collisions computed by the HHCM (long-dashed), the $\mathrm{HHCM}^{+\mathrm{cor}}$ (solid), the variational method (short-dashed) [4–6], and the 14-state CCA (dot-dashed) [11]. The variational and 14-state CCA results are from the figures in Ref. [5].

we computed the positronium formation cross section according to Eq. (16), $\sigma_{32}^L = [(2L+1)/k_3^2]|\tilde{S}_{32}^L|^2$, where k_3 is the wave vector of the incoming positron. In the HHCM calculation, the wave vector $K_\mu(R)$ defined by Eq. (8) is used for all values of R, real and complex.

In order to take into account the correction term to the HHCM, we also computed the Stuckelberg phase, probability, and positronium formation cross section using the wave vector $\tilde{K}_\mu(R)$ defined by Eq. (17) along the real axis ($R > R_2^t$) and $K_\mu(R)$ defined by Eq. (8) in the complex plane. We refer to these calculations as $\mathrm{HHCM}^{+\mathrm{cor}}$.

We present in Figs. 2–4, respectively, the *s*-, *p*- and *d*-wave positronium formation cross section computed with the HHCM and the $\mathrm{HHCM}^{+\mathrm{cor}}$ calculations and compare these calculations with variational [4–6] and 14-state CCA [11] calculations.

A. Results for the *s* wave

It has been known for over a decade from the variational results that the *s*-wave positronium formation cross section is small and has two minimum at $k=0.074$ and 0.31 [4]. The HHCM and the $\mathrm{HHCM}^{+\mathrm{cor}}$ calculations explain why the *s*-wave positronium formation cross section is small and the reason for a minimum. These calculations obtain a Stuckelberg phase close to, or equal to, π. This means the two amplitudes that correspond to different paths leading to positronium formation destructively interfere and that the corresponding *s*-wave cross section is nearly zero. In the HHCM calculation, the Stuckelberg phase goes through π at $k=0.26$ giving a minimum in the *s*-wave positronium formation cross section at this energy. In the $\mathrm{HHCM}^{+\mathrm{cor}}$ calculation, the Stuckelberg phase goes through π at a different energy, $k=0.08$, giving a minimum in the cross section. Interestingly, the position of the minimum in HHCM cross section is close to the second minimum in the variational calculation and the position of the minimum in the

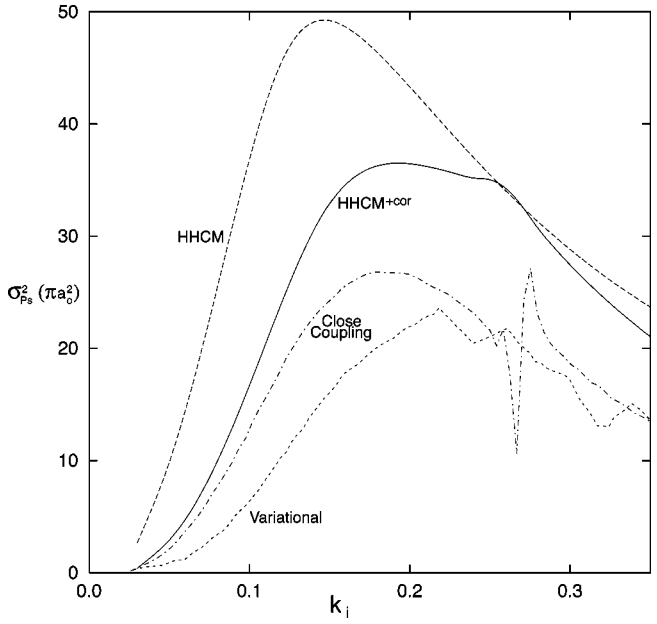

FIG. 4. The *d*-wave positronium formation cross section for $e^+ + \mathrm{Li}$ collisions computed by the HHCM (long-dashed), the $\mathrm{HHCM}^{+\mathrm{cor}}$ (solid), the variational method (short-dashed) [4–6], and the 14-state CCA (dot-dashed) [11]. The variational and 14-state CCA results are from the figures in Ref. [5].

$HHCM^{+cor}$ cross section is extremely close to the first minimum in the variational calculation.

Because the Stuckelberg phase is nearly π, the *s*-wave positronium formation cross section is very sensitive to the accuracy with which the phase is determined. This is reflected in the extreme sensitivity of the variational calculations to the choice of model potential, and the CCA calculations to the number of states and pseudostates included. Watts and Humberston [4] reported a factor of 10 difference between the *s*-wave positronium formation cross section computed with the two different model potentials. The *s*-wave elastic cross section and the *p*- and *d*-wave elastic and positronium formation cross sections showed significantly less sensitivity to the choice of the model potential. Kernoghan *et al.* [11] noted a factor of 1000 difference between their 8-state CCA and 14-state CCA calculations of the *s*-wave positronium formation cross section. The two sets of CCA calculations did not vary so dramatically for the *s*-wave elastic cross section and *p*- and *d*-wave elastic and positronium formation cross sections.

The HHCM and $HHCM^{+cor}$ calculations do not give the resonance that is seen in the 14-state CCA calculation [11]. The resonance occurs at a value of k close to the minimum in the HHCM and the second minimum in the variational results. The cause of this resonance is not known and it is not present in the 8-state CCA [11] or the variational [4–6] calculations. A noteworthy feature of the HHCM is that it does not seem to give rise to spurious resonances which can be a problem with CCA and Kohn variational methods.

The HHCM and $HHCM^{+cor}$ calculations have provided an interpretation of the *s*-wave positronium formation cross section results. Although the HHCM and the $HHCM^{+cor}$ calculations generally overestimates the cross section, they explain the reason for a minimum and the overall small magnitude of the cross section.

B. Results for the *p* wave

For the *p*-wave positronium formation cross section, the $HHCM^{+cor}$ results are in closer agreement in both shape and magnitude with the variational [5,6] and 14-state CCA [11] results than the HHCM results (Fig. 3). The position of the maximum in the $HHCM^{+cor}$ calculation ($k=0.07$) is in close agreement with the position of the maximum in the variational and 14-state CCA results ($k=0.08$). The HHCM overestimates the cross section compared to the variational results by a factor of 2 for $0.16 \leqslant k \leqslant 0.362$. The $HHCM^{+cor}$ cross section is a factor of 1.9 times larger than the variational results at $k=0.1$. However, with increasing k the agreement between the $HHCM^{+cor}$ and variational results significantly improves so that by $k=0.3$ the difference is less than 20%. This clearly illustrated the importance of including the $[1/4R^2+\langle \varphi_\mu(R)|\partial^2\varphi_\mu/\partial R^2\rangle]$ correction term [14] in the wave vector.

There is a slight barrier (3.4×10^{-4} a.u.) in the *p*-wave potential $\varepsilon_3'(R)$ used in the HHCM calculation. The HHCM cross section must be multiplied by the transmission modulus squared term $|T|^2$ associated with the barrier [14]. However, because the height of the barrier is extremely small, $|T|^2$ is close to unity and the barrier has negligible effect on the cross section away from threshold ($k<0.1$). As k approaches zero, $|T|^2$ tends to zero and this lowers the cross section dramatically.

For $k<0.11$, the $HHCM^{+cor}$ cross section is smaller than the HHCM cross section and in better accord with the variational and CCA calculations. The difference between the HHCM and $HHCM^{+cor}$ results, which is more significant with decreasing k, can primarily be attributed to the long-range behavior of the $e^+ + \mathrm{Li}(2s)$ potentials used in the calculations. For small k, $R_3^t < \mathrm{Re}(R_{23}^b)$. As k is decreased, R_3^t moves to larger R. The potential $\tilde{\varepsilon}_3'(R)$ lies slightly above the potential $\varepsilon_3'(R)$ for $R<1.1$. This has the effect that for very small k, R_3^t in the $HHCM^{+cor}$ calculation is significantly larger than in the HHCM calculation which means that one has to integrate over a longer range to compute the probability. This results in a smaller probability and a smaller cross section. The comparison of the HHCM and the $HHCM^{+cor}$ calculations for small k suggests that one should use the potential $\tilde{\varepsilon}_\mu'(R)$ for large R. There is little difference between the *p*-wave Stuckelberg phase computed between the two sets of calculations. For the HHCM, the Stuckelberg phase varies from 2.724 to 2.643 for the energy range 0–1.8 eV, whereas for the $HHCM^{+cor}$ calculation the Stuckelberg phase varies from 2.661 to 2.885.

C. Results for the *d* wave

By comparing the HHCM calculation of the *d*-wave positronium formation cross section with the 14-state CCA calculation [11] (Fig. 4), it can be seen that the HHCM has the main features of the cross section. The cross section tends to zero as the incident positron wave number is decreased towards the $\mathrm{Li}(2s)$ threshold. The maximum in the cross section is at $k=0.15$, slightly to left of the position of the maximum in the 14-state CCA calculation ($k=0.18$). The HHCM cross section is larger than the 14-state CCA cross section. For instance, the height of the maximum in the HHCM calculation is about twice the 14-state CCA calculation. (According to Watts [5] and Humberston [34] their *d*-wave variational results are not fully converged and therefore are probably significantly less accurate than the lower partial-wave variational results.) The HHCM and $HHCM^{+cor}$ calculations do not give the resonance seen in the 14-state CCA [11]. This resonance is also not present in the 8-state CCA [11] and its physical origin is not known.

The $HHCM^{+cor}$ calculation gives better agreement than the HHCM with the 14-state CCA calculation [11] for the *d*-wave positronium formation cross section. The position of the maximum ($k=0.19$) in the $HHCM^{+cor}$ calculation is in good agreement with the position of the maximum in the CCA calculation. The magnitude of the $HHCM^{+cor}$ cross section is generally smaller than the HHCM cross section. At the height of the maximum, the HHCM cross section is only about a factor of 1.4 times larger than the 14-state CCA calculation [11].

The *d*-wave Stuckelberg phase obtained in the HHCM and HHCM$^{+\mathrm{cor}}$ calculations varies from 1.960 to 2.104 and from 1.909 to 2.207, respectively.

V. CONCLUSION

The HHCM and HHCM$^{+\mathrm{cor}}$ calculations have provided an interpretation of the main features of the *s*-, *p*-, and *d*-wave positronium formation cross sections for positron-lithium collisions. For the *s* wave, obtaining a Stuckelberg phase close to π is an important finding because there are no examples of the Stuckelberg phase being an integer multiple of $\pi/2$ for electron collisions. There are, however, examples of the Stuckelberg phase being integer multiples of $\pi/2$ for other reactions. For example, Ward *et al.* [14] showed using the HHCM that the Stuckelberg phase is close to π for *s*-wave positronium formation in positron-hydrogen collisions and $\pi/2$ for the *d* wave. Ostrovsky [35] has noted Stuckelberg phases close to integer multiples of $\pi/2$ for the $L=0$ $dt\mu$ rearrangement process. In addition, Nielsen and Macek [15] have reported a Stuckelberg phase of 3π for low-energy recombination of identical bosons in three-body collisions. The reason why the Stuckelberg phase has a value equal to an integer multiple of $\pi/2$ for certain reactions at particular energies is not known. The present result together with the earlier results of Ward *et al.* [14] and Ostrovsky [35] shows the Stuckelberg phases of integer multiples of $\pi/2$ can be obtained for rearrangement processes.

For *s*-wave positronium formation in positron-lithium collisions, because the Stuckelberg phase is close to (or equal to) π, the cross section is very small (or zero) and highly sensitive to the accuracy with which the phase is determined. For the *p*- and the *d*-wave positronium formation cross sections, the HHCM$^{+\mathrm{cor}}$ calculation gives better agreement with the variational [4–6] and CCA [11] results than the HHCM calculation. The position of the HHCM$^{+\mathrm{cor}}$ maximum in the *p*- and the *d*-wave positronium formation cross sections agrees well with the variational [4–6] and CCA [11] calculations. It should be noted that both HHCM and HHCM$^{+\mathrm{cor}}$ calculations generally overestimates the positronium formation cross section for all partial waves. The correction term, previously derived asymptotically from the one-Sturmian theory [13,14], improves the HHCM results. These calculations therefore demonstrate the importance of including the correction term.

The HHCM and the HHCM$^{+\mathrm{cor}}$ results for low-energy positron-lithium collisions are encouraging and motivate a complete study of positron collisions with the alkali metals. The primary goal of this study is to provide insight into what causes the Stuckelberg phase to be integer multiple of $\pi/2$ The application of HHCM to positron–alkali-metal collisions will enable a systematic study of the dependency of the Stuckelberg phase on energy *E*, total orbital angular momentum *L*, and atomic number *Z* for the same atomic series.

ACKNOWLEDGMENTS

We are grateful for discussions with Dr. J. H. Macek and Dr. S. Yu. Ovchinnikov. We gratefully acknowledge support from the Institute for Theoretical Atomic and Molecular Physics at the Harvard-Smithsonian Center for Astrophysics. S.J.W. also acknowledges support from NSF under Grant No. PHY-9780016 and from UNT faculty research grants.

[1] C.E. Moore, *Atomic Energy Levels* Natl. Bur. Stand. (U.S.) Circ. No. 467, U.S. G.P.O., Washington, D.C., 1949), Vol. 1.
[2] E.P. Wigner, Phys. Rev. **73**, 1002 (1948).
[3] E. Surdutovich, J.M. Johnson, W.E. Kauppila, C.K. Kwan, and T.S. Stein, Phys. Rev. A **65**, 032713 (2002).
[4] M.S.T. Watts and J.W. Humberston, J. Phys. B **25**, L491 (1992).
[5] M.S.T. Watts, Ph.D. thesis, University of London, 1994.
[6] J.W. Humberston and M.S.T. Watts, Hyperfine Interact. **89**, 47 (1994).
[7] S. Guha and A.S. Ghosh, Phys. Rev. A **23**, 743 (1981).
[8] M. Basu and A.S. Ghosh, Phys. Rev. A **43**, 4746 (1991).
[9] R.N. Hewitt, C.J. Noble, and B.H. Bransden, J. Phys. B **25**, 2683 (1992).
[10] R.N. Hewitt, C.J. Noble, and B.H. Bransden, Hyperfine Interact. **89**, 195 (1994).
[11] A.A. Kernoghan, M.T. McAlinden, and H.R.J. Walters, J. Phys. B **27**, L625 (1994).
[12] M.T. McAlinden, A.A. Kernoghan, and H.R.J. Walters, J. Phys. B **30**, 1543 (1997).
[13] J.H. Macek and S.Yu. Ovchinnikov, Phys. Rev. A **54**, 544 (1996).
[14] S.J. Ward, J.H. Macek, and S.Yu. Ovchinnikov, Phys. Rev. A **59**, 4418 (1999).
[15] E. Nielsen and J.H. Macek, Phys. Rev. Lett. **83**, 1566 (1999).
[16] J.H. Macek, S.Yu. Ovchinnikov, and S.V. Pasovets, Phys. Rev. Lett. **74**, 4631 (1995).
[17] J.H. Macek and W. Ihra, Phys. Rev. A **55**, 2024 (1997).
[18] W. Ihra, F. Mota-Furtado, P.F. O'Mahony, and J.H. Macek, Phys. Rev. A **55**, 3250 (1997).
[19] W. Ihra, J.H. Macek, F. Mota-Furtado, and P.F. O'Mahony, Phys. Rev. Lett. **78**, 4027 (1997).
[20] N. Miyashita, S. Watanabe, M. Matsuzawa, and J.H. Macek, Phys. Rev. A **61**, 014901 (1999).
[21] G. Gasaneo and J.H. Macek, J. Phys. B **35**, 2239 (2002).
[22] L.D. Landau and E.M. Lifshitz, *Quantum Mechanics: Non-Relativistic Theory* (Pergamon Press, Oxford, 1981), Chap. 7, 164ff.
[23] Y. Zhou and C.D. Lin, J. Phys. B **27**, 5065 (1994).
[24] Yu. Demkov, in *Proceedings of Invited Talks of the XI International Conference on the Physics of Electronic and Atomic Collisions*, Leningrad, 1967, edited by I.P. Flaks and E.A. Solov'ev (Joint Institute for Laboratory Astrophysics, Boulder, CO, 1968), p. 186.
[25] S.V. Passovets, J.H. Macek, and S.Yu. Ovchinnikov, in *The Physics of Electronic and Atomic Collisions*, edited by Louis. J. Dubé, J. Brian A. Mitchell, J. William McKonkey, and Chris

E. Brion, AIP Conf. Proc. 360 (AIP, Woodbury, NY, 1995), p. 347.
[26] J.H. Macek and X.Y. Dong, Nucl. Instrum. Methods Phys. Res. B **42**, 475 (1989).
[27] E.E. Nikitin and S.Yu. Umanskii, *Theory of Slow Atomic Collisions* (Springer-Verlag, Berlin, 1984).
[28] J. Macek, J. Phys. B **1**, 831 (1968).
[29] Z. Zhen and J. Macek, Phys. Rev. A **34**, 838 (1986).
[30] M. Cavagnero, Z. Zhen, and J. Macek, Phys. Rev. A **41**, 1225 (1990).
[31] G. Peach, H.E. Saraph, and M.J. Seaton, J. Phys. B **21**, 3669 (1988).
[32] K.J. Bathe, *Finite Element Procedures* (Prentice-Hall, New Jersey, 1996).
[33] Y. Zhou, C.D. Lin, and J. Shertzer, J. Phys. B **26**, 3937 (1993).
[34] J.W. Humberston (private communication).
[35] V.N. Ostrovsky, Phys. Rev. A **61**, 032505 (2000).